Field-free molecular orientation by femtosecond dual-color and single-cycle THz fields

Hao Li, Wenxue Li,* Yahui Feng, Haifeng Pan, and Heping Zeng†
State Key Laboratory of Precision Spectroscopy, East China Normal University, Shanghai 200062, China
(Received 15 June 2013; published 26 July 2013)

We theoretically demonstrate the dynamics of field-free molecular orientation under the radiation of a femtosecond dual-color field and a delayed single-cycle terahertz (THz) field, with CO and LiH as the prototype molecules. The results show that the impulsive Raman processes of dual-color field and the resonant effect of the THz field exhibit higher excitation efficiency in a combined way and give rise to a significant enhancement of orientation degree when the THz field is introduced around the full revival time of molecules. It also shows that the dual-color field has an advantage over the single-color field when they combine with the THz field in creating field-free orientation.

DOI: 10.1103/PhysRevA.88.013424 PACS number(s): 37.10.Vz, 33.80.−b, 32.80.Qk, 42.50.Hz

I. INTRODUCTION

Alignment [1,2] and orientation [3,4] of gas-phase molecules have long been noted to play a critical role in many physical and chemical processes, such as high-harmonic generation (HHG) [5], strong field ionization and dissociation [6], spectral manipulation [7,8], chemical reaction control [9], functional material construction [10], and so on. Alignment, for both nonpolar and polar molecules, refers to the confinement of molecular axes to a fixed direction, such as the polarization of external field, whereas orientation, mainly for polar molecules, has further specific "head-versus-tail" order, which requires that the molecular rotational wave function lies in the coherent superposition of even J (even parity) and odd J (odd parity) states. As molecules in the Boltzmann distribution condition initially occupy a single even or odd J state, it needs extra manipulation to change the parity of the initial wave function. Thus far, several methods have been proposed for orientation. It was demonstrated that a few-cycle THz pulse [11–15] can be used to generate effective molecular orientation. Actually, the solution of the THz field has to be zero area, i.e., $\int \varepsilon(t)dt = 0$. Such characteristic arises from the requirement of Maxwell equations, and thus the THz electric field can be asymmetric, with a narrow but intense positive peak and long but weak negative tails. The THz field changes the parity of rotational wave function via interacting with the molecular permanent dipole moment, and its advantage lies in the fact that the transition frequency between rotational states generally stays in THz or sub-THz range so that the resonant THz-molecule interaction shows a higher efficiency. Alternatively, owing to the advancement of laser technology, the peak intensity of the focused femtosecond laser pulse can steadily reach the order of 10^{13} W/cm^2, by which the dual-color laser field gradually becomes a promising tool for achieving molecular orientation [16–18]. Dual-color field also exhibits the feature of asymmetry. Its interaction with molecular hyperpolarizability changes the parity of rotational wave function through three-photon Raman transition [3]. Moreover, because the maximum degree of orientation by a single pulse is strictly limited by its peak intensity and temporal duration, it is highly desired to develop multipulse schemes to obtain improved results. Fortunately, the present femtosecond technology allows much more complex optical modulation for the orienting molecule, such as controllable delay between two dual-color pulses [19], slow rising and rapid falling of pulse edges [20], and the combination of single-color and THz pulses [21]. Since both the dual-color field and the THz field have their respective advantages, it is significant to apply them at the same time. Interestingly, the dual-color pulse has a relative lower critical power for the femtosecond filamentation process [22] so that it can easily generate femtosecond filaments. When a dual-color pulse undergoes filamentation, the field intensity in the optical filament stabilizes around 5×10^{13} W/cm^2 [22], accompanying which there automatically follows a resonant enhancement of plasma generation and an enhanced THz wave emission [23–25]. Therefore, it should be an interesting way to make full use of the features of dual-color and THz fields simultaneously.

In this paper, we investigate the dynamics of orientation under the excitation of dual-color and THz fields, with a controllable delay time. The discussions cover the cases of molecules with a longer revival period T_{Rev} (CO), as well as a shorter one (LiH). We show that the combination of the dual-color and THz fields makes full use of their advantages and gives rise to an enhancement of orientation if the THz field is applied around the full revival time of the molecules. Meanwhile, comparing with the combination of single-color and THz fields [21], our scheme also shows improved excitation efficiency and higher orientation Degrees.

II. THEORETICAL ANALYSIS

We consider that a polar molecule is subjected to linearly polarized dual-color and THz laser pulses, as shown in Fig. 1(a), given by

$$\begin{aligned}\varepsilon(t) &= \varepsilon_{\mathrm{DC}}(t) + \varepsilon_{\mathrm{THz}}(t + T_d, \varphi_{\mathrm{CEP}}) \\ &= \exp[-(t/\tau_{\mathrm{DC0}})^2][\varepsilon_\omega \cos(\omega t) + \varepsilon_{2\omega} \cos(2\omega t)] \\ &\quad + \exp\{-[(t + T_d)/\tau_{\mathrm{THz0}}]^2\}\varepsilon_{\mathrm{THz}} \cos[\omega_{\mathrm{THz}}(t + T_d) \\ &\quad + \varphi_{\mathrm{CEP}}], \end{aligned} \tag{1}$$

where $\tau_{\mathrm{DC0(THz0)}} = \tau^{\mathrm{FWHM}}_{\mathrm{DC(THz)}}/\sqrt{2\ln 2}$ is the pulse duration, ω and 2ω are the carrier frequencies of the fundamental and

*wxli@phy.ecnu.edu.cn
†hpzeng@phy.ecnu.edu.cn

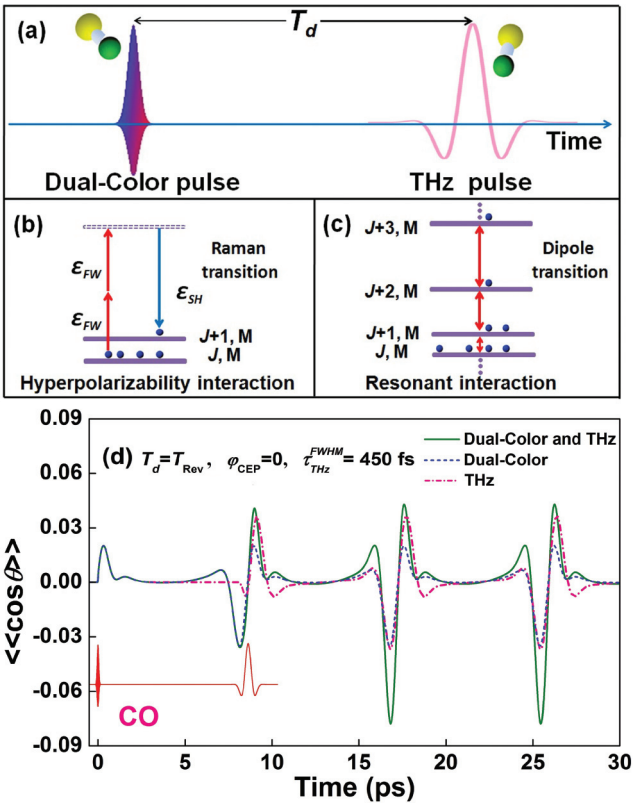

FIG. 1. (Color online) (a) Schematicillustration of the molecular orientation excited by femtosecond dual-color field and single-cycle THz field. T_d denotes the time delay between the peaks of dual-color and THz fields. (b) and (c) show the hyperpolarizability interaction and resonant interaction induced by dual-color field and THz field, respectively. (d) The field-free orientation of CO by THz field (pink dash-dot line), dual-color field (blue dash line), and their combined fields (olive solid line). The inset line shows the timing sequence of combined fields.

second harmonic waves, while $\varphi_{\rm CEP}$ and T_d denote the carrier-envelope phase (CEP) of $\varepsilon_{\rm THz}$ and the time delay between $\varepsilon_{\rm DC}$ and $\varepsilon_{\rm THz}$. The field-molecule interaction is closely related to the molecular constants as

$$\begin{aligned} H(t) &= H_0 + V_\mu(\theta)\varepsilon(t) + V_{\rm pol}(\theta)\varepsilon^2(t) + V_{\rm hyp}(\theta)\varepsilon^3(t) \\ &= B_0 J^2 - \mu_0\varepsilon(t)\cos\theta - 1/2[(\alpha_\parallel - \alpha_\perp)\cos^2\theta + \alpha_\perp] \\ &\quad \times \varepsilon^2(t) - 1/6[(\beta_\parallel - 3\beta_\perp)\cos^3\theta + 3\beta_\perp\cos\theta]\varepsilon^3(t), \end{aligned} \tag{2}$$

where B_0, J, μ_0, and ε denote the rotational constant, rotational angular momentum operator, permanent dipole moment, and the applied field, respectively, while $\alpha_\parallel(\beta_\parallel)$ and $\alpha_\perp(\beta_\perp)$ represent the polarizability (hyperpolarizability) components parallel and perpendicular to the main molecular axis. The calculation of orientation is divided into the field-on step and field-off step. In the field-on step, for any specific initial rotational state $\psi(t=0) = |J_0M_0\rangle$, with the laser-molecule interaction going on, as shown in Figs. 1(b) and 1(c), the wave function coherently evolves into the superposition of a series of field-free rotors' eigenfunctions by Raman transition [3] or resonant dipole transition as follows:

$$\psi(t) = \sum d_{JM}(t)|JM\rangle, \tag{3}$$

whose time-dependent complex coefficient $d_{JM}(t)$ can be determined by solving the time-dependent Schrödinger equation (see Appendix for details),

$$i\hbar\partial\psi(t)/\partial t = H(t)\psi(t). \tag{4}$$

In the field-off step, the wave packets freely evolve as

$$\psi(t) = \sum_{JM} d_{JM}\exp\left(-i\frac{E_J}{\hbar}t\right)|JM\rangle = \sum_{JM} c_{JM}(t)|JM\rangle, \tag{5}$$

where $E_J = B_0J(J+1)$ is the rotational energy of the field-free rotor in J state. The complex coefficients $c_{JM}(t)$ contain all information about the wave packet, such as population of each J state in Eq. (5). With the time-dependent $c_{JM}(t)$, the contribution of the initial state $|J_0M_0\rangle$ to orientation degree can be calculated by

$$\langle\cos\theta(t)\rangle_{J_0M_0} = \sum_{JM,J'M'} c^*_{JM}(t)c_{J'M'}(t)\langle JM|\cos\theta|J'M'\rangle \tag{6}$$

It has been pointed out that the value of $\langle\cos\theta(t)\rangle_{J_0M_0}$ reaches its maximum when the coherent wave packet in Eq. (5) evolves into the state in which the total population of even J is equal to that of odd J [21]. If the initial state $|J_0M_0\rangle$, which populates in a single even or odd J state, is sufficiently excited into a coherent wave packet with equal even and odd populations, this must be accompanied by significant variations in population, and hence the condition of population is critical for characterizing molecular orientation. As the initial rotational states of the molecular ensemble in thermal equilibrium follow a Boltzmann distribution, the total contributions of various initial rotational states should be weighted in average as

$$\begin{aligned} \langle\!\langle\cos\theta(t)\rangle\!\rangle &= \sum_{JM} w_J\langle\cos\theta(t)\rangle_{JM} \\ &= \frac{\sum_{JM}\exp(-E_J/kT)\langle\cos^2\theta(t)\rangle_{JM}}{\sum_J(2J+1)\exp(-E_J/kT)}, \end{aligned} \tag{7}$$

where w_J is the Boltzmann weight factor and T is the initial temperature of the molecular ensemble.

III. RESULTS AND DISCUSSIONS

A. The case of CO molecule

In our calculation, the relevant parameters for the dual-color pulse are $\tau_{\rm DC}^{\rm FWHM} = 35$ fs, $\lambda_\omega = 800$ nm, $\lambda_{2\omega} = 400$ nm, $I_\omega + I_{2\omega} = 5\times10^{13}$ W/cm^2, and the ratio $I_\omega : I_{2\omega}$ is chosen as an optimized value of 2 [17], while for the THz field $\tau_{\rm THz}^{\rm FWHM} = 450$ fs, $\omega_{\rm THz} = 2\pi\times10^{12}$ Hz, and its peak field strength $\varepsilon_{\rm THz}$ is taken as 3 MV/cm, which is a typical order of magnitude for creating effective orientation. The initial temperature T is kept as 30 K. We firstly take the CO molecule as an example, whose parameters are $\mu_0 = 3.734\times10^{-31}$ C m, $B_0 = 3.83\times10^{-23}$ J, $\alpha_\parallel = 2.553\times10^{-40}$ C^2 m^2 J^{-1}, $\alpha_\perp = 1.969\times10^{-40}$ C^2 m^{2}J^{-1}, $\beta_\parallel = 1.02\times10^{-51}$ C^3 m^3 J^{-2}, $\beta_\perp = 1.85\times10^{-52}$ C^3 m^3 J^{-2} [26]. These parameters are sometimes

given in atomic units or electrostatic units in some studies. Their conversion factors to SI units are listed here for convenience. 1 a.u. of $\mu \approx 2.542$ D $\approx 8.478 \times 10^{-30}$ C m; 1 a.u. of $\alpha \approx 0.148$ Å$^3 \approx 1.649 \times 10^{-41}$ C^2 m^2 J^{-1}; 1 a.u. of $\beta \approx 8.638 \times 10^7$ Å$^5 \approx 3.206 \times 10^{-53}$ C^3 m^3 J^{-2}; 1 a.u. of $E \approx 2.195 \times 10^5$ cm$^{-1} \approx 4.359 \times 10^{-18}$ J.

Figure 1(d) shows the temporal evolution of the field-free orientation of the CO molecule after the excitations of the THz field (pink dash-dot line), dual-color field (blue dash line), and their combination (olive solid line), respectively, with $T_d = T_{\mathrm{Rev}} = 8.64$ ps and $\varphi_{\mathrm{CEP}} = 0$. Here, positive $\langle\langle \cos\theta \rangle\rangle$ corresponds to the case when carbon atoms point upwards. Comparing with the separated ways, the generated orientation degree in the combined way is enhanced by a factor of about 2 when the THz field is applied around T_{Rev}. Due to the robustness of orientation, the enhancement remains valid for the moderate changes of temperature as well as the intensities of the fields, which is critical for experimental applications. For the property of periodic evolution, the rotational wave function around T_{Rev} is the exact copy around zero delay, just after the excitation of the dual-color field. As shown by the timing sequence of the fields in Fig. 1(d), when the wave function starts a new period at T_{Rev}, the in-phase THz field strikes the molecules to orient to the positive direction, as the dual-color field did around zero delay. Therefore, in the impulse limit, the extra in-phase kick of the THz field promotes the orientation, although the negative part of the zero-area THz field actually acts in an opposite way to degrade the promotion. The enhancement can also be explained by the fact that, based on the preexcitation of the dual-color field, if the in-phase THz field is applied at T_{Rev}, it would play a role in strengthening the transition and coupling between even and odd J states of the precreated coherent wave packets [19], and consequently generates an enhanced field-free orientation.

Recently, it was demonstrated that the molecules prealigned by an intense 800-nm femtosecond pulse centered at 800 nm could be well oriented by the subsequent delayed THz field [21,27]. In this scheme, the intense single-color field effectively excites the molecules into higher J states so that the weaker THz field could avoid directly exciting the initial states into higher J states by the multiphoton process. Here, we make a simple comparison. In Fig. 2(a), the orange squares (violet circles) show the maximum orientation degree created by dual-color (single-color) field and delayed THz field, with the delay time T_d varying from zero to about $2T_{\mathrm{Rev}}$. The parameters used for the dual-color and THz fields are identical with those in Fig. 1(d). For single-color field, in order to be comparable, we kept its FWHM duration $\tau_{\mathrm{SC}}^{\mathrm{FWHM}} = 35$ fs, central wavelength $\lambda_\omega = 800$ nm, and peak intensity $I_\omega = 5.0 \times 10^{13}$ W/cm^2. Figure 2(a) shows that the dual-color scheme exhibits an apparent advantage over the single-color scheme in orienting molecules. This is because the single-color field creates a coherent wave packet according to the selection rule of $\Delta J = 0, \pm 2$ so that its prealignment fails to break the parity of wave function until the arrival of the THz field, and hence lowers the excitation efficiency. By contrast, the dual-color field is capable of directly exciting the initial states into coherent superposition states consisting of both even and odd J states. In Fig. 2(b), the green (light gray) bars [red (dark gray) bars] show the population in various J states after the excitation of dual-color (single-color) and THz fields. For $J = 0$–3, their populations in the single-color scheme are larger than those in the dual-color scheme, whereas the conditions for higher J from 4 to 9 are the reverse. It also suggests that the preorientation of the dual-color field shows higher excitation efficiency. Therefore, when cooperating with the THz field, the dual-color field has an advantage over the single-color field in creating orientation for its characteristic of asymmetry.

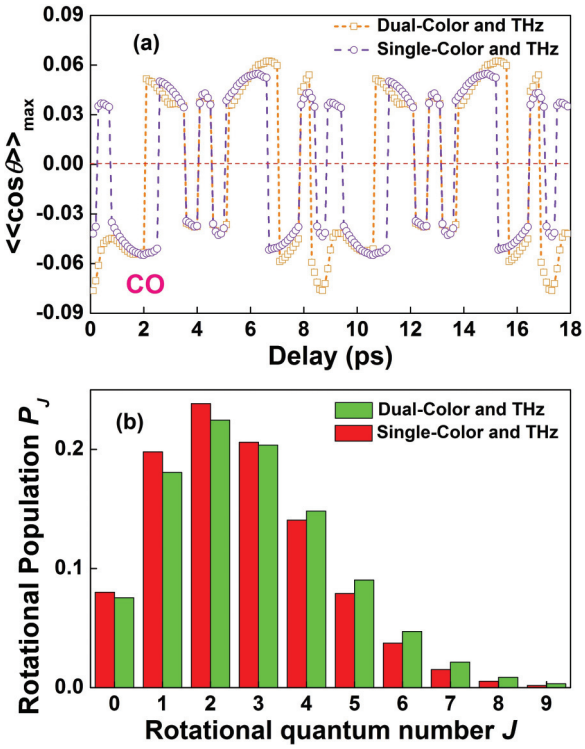

FIG. 2. (Color online) (a) The orange squares (violet circles) show the maximum degree of field-free orientation created by dual-color (single-color) field and delayed THz field at various T_d, with $\varphi_{\mathrm{CEP}} = 0$. (b) The green bars (red bars) show the populations of rotational states of CO, after the excitation of dual-color (single-color) and THz fields.

B. The case of LiH molecule

In the case of the LiH molecule, the parameters used are $\mu_0 = 1.958 \times 10^{-29}$ C m [28], $B_0 = 1.493 \times 10^{-22}$ J, $\alpha_\parallel = 4.254 \times 10^{-40}$ C^{2}m^{2}J^{-1}, $\alpha_\perp = 4.881 \times 10^{-40}$ C^{2}m^{2}J^{-1}, $\beta_\parallel = 2.019 \times 10^{-50}$ C^3 m^{3}J^{-2}, $\beta_\perp = 7.502 \times 10^{-51}$ C^{3}m^{3}J^{-2} [29]. Comparing with the CO molecule, LiH has a shorter revival period ($T_{\mathrm{Rev}} = 2.22$ ps) but much greater optical nonlinearity, which leads to a larger orientation degree as well as many other new features. The parameters for dual-color or THz fields are the same as above unless otherwise specified. In Fig. 3(a), it shows the molecular orientation created by dual-color field (blue dash line) and the combined fields (olive solid line), with $T_d = T_{\mathrm{Rev}}$ and $\varphi_{\mathrm{CEP}} = 0$. Here, positive molecular orientation is defined by the case that Li atoms are directed upwards. The blue dash line presents a clear periodic feature of field-free orientation,

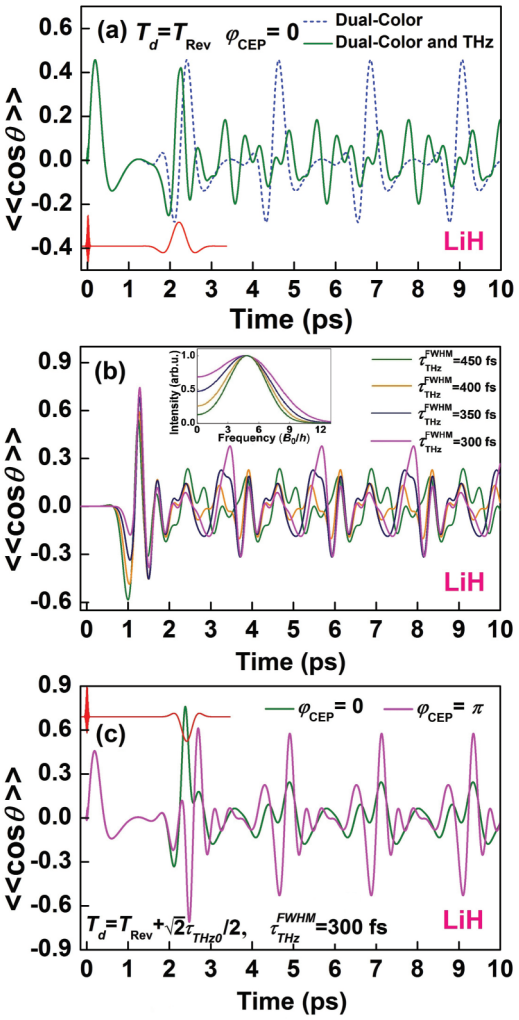

FIG. 3. (Color online) (a) Molecular orientation created by dual-color field (blue dash line) and the combined fields (olive solid line), with $T_d = T_{\mathrm{Rev}}$, $\varphi_{\mathrm{CEP}} = 0$. (b) Molecular orientation created by THz fields with various pulse durations. (c) Molecular orientation created by combined fields, with $T_d = 2.41$ ps ($T_d = T_{\mathrm{Rev}} + \sigma_{\mathrm{THz0}}/2 = T_{\mathrm{Rev}} + \sqrt{2}\tau_{\mathrm{THz0}}/2$, $\sigma_{\mathrm{THz0}} = \sqrt{2}\tau_{\mathrm{THz0}}$, is the duration of electric field), and $\varphi_{\mathrm{CEP}} = 0$ (olive line), $\varphi_{\mathrm{CEP}} = \pi$ (pink line).

with the maximum orientation being 0.44. However, when the delayed THz field is applied, the evolution of orientation changes with the electric field. After the extinction of the THz field, it ends up with a poor field-free orientation. Obviously, the evolution exhibits a typical characteristic of adiabatic excitation [1] rather than the field-free condition when the THz field is present. It suggests that, in the case of short revival time, the relatively longer THz-molecule interaction cannot be taken as a "kick." The impulse limit, in which the interaction is supposed to be instantaneous on the scale of the rotational period, is valid only when $\tau_0 \ll T_{\mathrm{Rev}}$ [30,31], so that here its requirement cannot be satisfied any more. Figure 3(b) presents the molecular orientations created by THz fields with different pulse durations. It is found that shorter THz fields create higher field-free orientations. The reason lies in the fact that as the pulse duration of the THz field gets shorter, the asymmetric characteristic of its electric field becomes more prominent. It is also consistent with the fact that a shorter THz field holds a broader spectrum, as shown in the inset of Fig. 3(b), which enables it to cover more rotational energy levels and create a higher field-free orientation degree.

Since the duration of the THz field cannot be neglected any longer, the delay time T_d must add another $\sigma_{\mathrm{THz0}}/2$ ($\sigma_{\mathrm{THz0}} = \sqrt{2}\tau_{\mathrm{THz0}}$ is the duration of the electric field) to ensure the beginning of the THz-molecule interaction occurs at T_{Rev} so that most of the THz field could contribute to the generation of orientation. In Fig. 3(c), it shows that the combined fields create a poor field-free orientation when $\varphi_{\mathrm{CEP}} = 0$, whereas in the case of $\varphi_{\mathrm{CEP}} = \pi$, it gives rise to a high-degree field-free orientation peaking at 0.60, with $T_d = T_{\mathrm{Rev}} + \sigma_{\mathrm{THz0}}/2 = T_{\mathrm{Rev}} + \sqrt{2}\tau_{\mathrm{THz0}}/2 = 2.41$ ps. The reason for such significant difference can be revealed by analyzing the temporal evolution of related rotational states. Figure 4 shows the populations of the main populated J states during the whole field-on step. The variations around zero delay and T_d are attributed to the dual-color field and the THz field, respectively. The incidence of dual-color field always causes drastic jitter, as shown by the inset in Fig. 4(a). Such feature is caused by the strong hyperpolarizability and alignment interactions, which induce not only $\Delta J = \pm 1$, $\Delta J = \pm 3$, but also $\Delta J = \pm 2$ transitions (see Appendix and [29]), and thus leads to complex transition paths and rapid variations of populations. The influence of

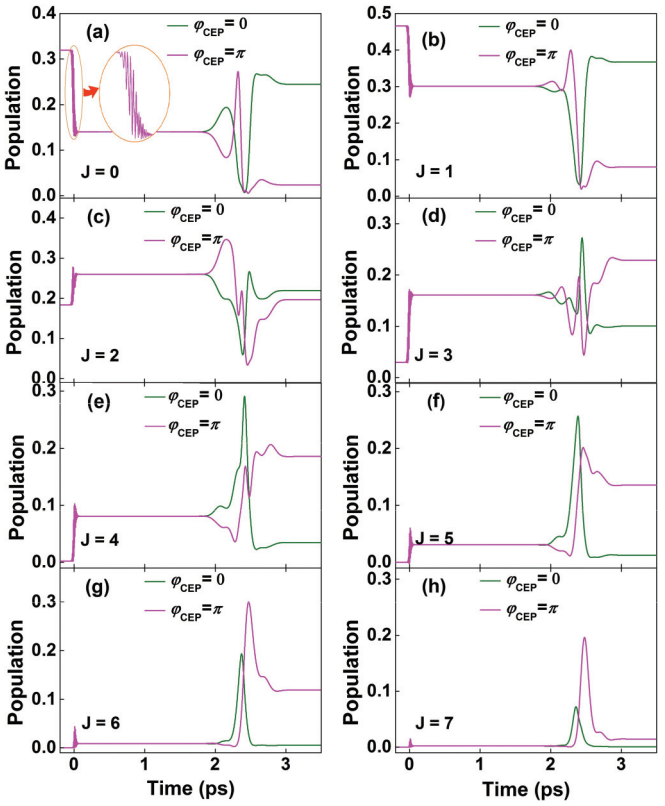

FIG. 4. (Color online) (a)–(h) show the temporal evolution of populations of main populated J states under the combined fields as used in Fig. 3(c), with $T_d = 2.41$ps, and $\varphi_{\mathrm{CEP}} = 0$ (olive line), $\varphi_{\mathrm{CEP}} = \pi$ (pink line).

the THz field is also profound. When the coherent wave packets created by the dual-color field are irradiated by the delayed THz field, the transition amplitude from J to $J+1$ is predicted to be [32]

$$A_{J,J+1}(t) \propto \frac{\mu_{J,J+1}}{i\hbar}(P_J - P_{J+1}) \int_{-\infty}^{t} \varepsilon_{\mathrm{THz}}(t') e^{i\Delta\omega_{J,J+1}t'} dt', \tag{8}$$

where $\mu_{J,J+1} = \mu_0 \langle J|\cos\theta|J+1\rangle$ is the dipole moment matrix element, $P_{(J)J+1}$ is the population of the J $(J+1)$ state, and $\Delta\omega_{J,J+1} = (E_{J+1} - E_J)/\hbar = 2B_0(J+1)/\hbar$ is the angular frequency spacing between neighboring J states. Therefore, for $\varphi_{\mathrm{CEP}} = 0$ and $\varphi_{\mathrm{CEP}} = \pi$, opposite THz electric fields induce different transitions and evolutions. In the case of $\varphi_{\mathrm{CEP}} = 0$, the populations in lower J ($J = 0, 1, 2$) roughly decrease first while those of higher J (J = 3–7) increase, and consequently there exists a peak orientation of 0.76 at 2.38 ps in Fig. 3(c). Such enhancement by the in-phase THz field is just similar to the case of CO in Fig. 1(d). The pulse duration of the THz field here is short enough for CO, but this is not true for LiH. After the peak orientation, the rest of the THz field induces a subsequent drop of higher J populations, which corresponds to the coherent transfer from $J+1$ states to J states, and finally results in the depletion of populations in higher J states and the accumulation in lower J states. On the contrary, in the case of $\varphi_{\mathrm{CEP}} = \pi$, the processes are generally the opposite, the deexcitation of higher J states occurs first and then is followed by a rise, ending up with more populations occupying higher J states, which suggests that, at the end of THz field, the coherent wave packets lie in the condition of being sufficiently excited, as discussed in Sec. II, and thus it gives rise to a higher field-free molecular orientation.

IV. CONCLUSION

In conclusion, we have analyzed the molecular orientation characteristics of polar molecules driven by a dual-color femtosecond laser field and a delayed single-cycle THz field. The scheme effectively combines the advantages of dual-color and THz fields together. The results indicate that an enhanced molecular orientation degree could be achieved for molecules with longer or shorter revival periods. This scheme is also applicable to other polar molecules in a considerable range of temperature and driving fields' intensities, and is expected to be beneficial to the research and applications of field-free molecular orientation in all related fields.

ACKNOWLEDGMENTS

This work was funded by New Scholar Prize (Grant No. MXRZZ2012005), National Basic Research Program of China (Grant No. 2011CB808105), National Key Scientific Instrument Project (Grant No. 2012YQ150092), National Natural Science Fund of China (Grants No. 11004061, No. 11274115, and No. 10990101), and International Science and Technology Collaboration Program (Grants No. 2010DFA04410 and No. 11530700900).

APPENDIX

By expanding Eq. (4) into explicit form with Eqs. (1)–(3), we obtain a set of coupled differential equations,

$$\begin{aligned} i\frac{\hbar}{B_0}\dot{d}_J(t) = {} & d_J(t)\frac{E_J}{B_0} - \omega_1(t)\sum_{J'} d_{J'}(t)\langle JM|\cos\theta|J'M\rangle \\ & - \omega_2(t)\sum_{J'} d_{J'}(t)\langle JM|\cos^2\theta|J'M\rangle \\ & - \omega_3(t)\sum_{J'} d_{J'}(t)\langle JM|\cos^3\theta|J'M\rangle, \end{aligned} \tag{A1}$$

where $\omega_1(t) = [\beta_\perp \varepsilon^3(t) + 2\mu_0\varepsilon(t)]/(2B_0)$, $\omega_2(t) = \Delta\alpha\varepsilon^2(t)/(2B_0)$, and $\omega_3(t) = (\beta_\parallel - 3\beta_\perp)\varepsilon^3(t)/(6B_0)$ are dimensionless coefficients. The nonvanishing matrix elements of the ω_1 and ω_2 terms in Eq. (A1) could be explicitly expressed by [33,34]

$$\langle J,M|\cos\theta|J' = J+1, M\rangle = \sqrt{\frac{(J+1)^2 - M^2}{(2J+1)(2J+3)}}, \tag{A2}$$

$$\langle J,M|\cos\theta|J' = J-1, M\rangle = \sqrt{\frac{J^2 - M^2}{(2J-1)(2J+1)}}, \tag{A3}$$

$$\langle J,M|\cos^2\theta|J' = J, M\rangle = \frac{(J+1)^2 - M^2}{(2J+1)(2J+3)} + \frac{J^2 - M^2}{(2J-1)(2J+1)}, \tag{A4}$$

$$\langle J,M|\cos^2\theta|J' = J+2, M\rangle = \sqrt{\frac{[(J+2)^2 - M^2][(J+1)^2 - M^2]}{(2J+1)(2J+3)^2(2J+5)}} \tag{A5}$$

$$\langle J,M|\cos^2\theta|J' = J-2, M\rangle = \sqrt{\frac{[(J-1)^2 - M^2](J^2 - M^2)}{(2J-3)(2J-1)^2(2J+1)}}. \tag{A6}$$

For the ω_3 term, considering that $\sum_{J''} |J''M\rangle\langle J''M| = 1$, the matrix element $\langle JM|\cos^3\theta|J'M\rangle$ could be expanded as follows:

$$\begin{aligned} \langle JM|\cos^3\theta|J'M\rangle = {} & \langle JM|\cos^2\theta \sum_{J''} |J''M\rangle\langle J''M|\cos\theta|J'M\rangle \\ = {} & [\langle JM|\cos^2\theta|J'' = J, M\rangle + \langle JM|\cos^2\theta|J'' = J+2, M\rangle + \langle JM|\cos^2\theta|J'' = J-2, M\rangle] \\ & \times [\langle J'' = J'+1, M|\cos\theta|J'M\rangle + \langle J'' = J'-1, M|\cos\theta|J'M\rangle]. \end{aligned} \tag{A7}$$

Therefore, with (A2)–(A6), there are six nonvanishing elements in Eq. (A7):

$$\langle J,M|\cos^2\theta|J''=J,M\rangle\langle J'',M|\cos\theta|J'=J''+1=J+1,M\rangle, \tag{A8}$$

$$\langle J,M|\cos^2\theta|J''=J,M\rangle\langle J'',M|\cos\theta|J'=J''-1=J-1,M\rangle, \tag{A9}$$

$$\langle J,M|\cos^2\theta|J''=J+2,M\rangle\langle J'',M|\cos\theta|J'=J''+1=J+3,M\rangle, \tag{A10}$$

$$\langle J,M|\cos^2\theta|J''=J+2,M\rangle\langle J'',M|\cos\theta|J'=J''-1=J+1,M\rangle, \tag{A11}$$

$$\langle J,M|\cos^2\theta|J''=J-2,M\rangle\langle J'',M|\cos\theta|J'=J''+1=J-1,M\rangle, \tag{A12}$$

$$\langle J,M|\cos^2\theta|J''=J-2,M\rangle\langle J'',M|\cos\theta|J'=J''-1=J-3,M\rangle. \tag{A13}$$

By far, all terms in Eq. (4) are explicit for calculation.

[1] H. Stapelfeldt and T. Seideman, Rev. Mod. Phys. **75**, 543 (2003).
[2] T. Seideman and E. Hamilton, Adv. At. Mol. Opt. Phys. **52**, 289 (2005).
[3] M. J. J. Vrakking and S. Stolte, Chem. Phys. Lett. **271**, 209 (1997).
[4] M. Machholm and N. E. Henriksen, Phys. Rev. Lett. **87**, 193001 (2001).
[5] R. Velotta, N. Hay, M. B. Mason, M. Castillejo, and J. P. Marangos, Phys. Rev. Lett. **87**, 183901 (2001).
[6] I. V. Litvinyuk, Kevin F. Lee, P. W. Dooley, D. M. Rayner, D. M. Villeneuve, and P. B. Corkum, Phys. Rev. Lett. **90**, 233003 (2003).
[7] J. Liu, Y. Feng, H. Li, P. Lu, H. Pan, J. Wu, and H. Zeng, Opt. Express **19**, 40 (2011).
[8] H. Li, W. Li, Y. Feng, J. Liu, H. Pan, and H. Zeng, Phys. Rev. A **85**, 052515 (2012).
[9] D. Hershbach, Rev. Mod. Phys. **71**, S411 (1999).
[10] M. B. Feller, W. Chen, and Y. R. Shen, Phys. Rev. A **43**, 6778 (1991).
[11] S. Fleischer, Y. Zhou, R. W. Field, and K. A. Nelson, Phys. Rev. Lett. **107**, 163603 (2011).
[12] J. Yang, M. Chen, J. Yu, and S.L. Cong, Eur. Phys. J. D **66**, 102 (2012).
[13] J. Ortigoso, J. Chem. Phys. **137**, 044303 (2012).
[14] M. Lapert and D. Sugny, Phys. Rev. A **85**, 063418 (2012).
[15] S. L. Liao, T. S. Ho, H. Rabitz, and Shih-I Chu, Phys. Rev. A **87**, 013429 (2013).
[16] T. Kanai and H. Sakai, J. Chem. Phys. **115**, 5492 (2001).
[17] R. Tehini and D. Sugny, Phys. Rev. A **77**, 023407 (2008).
[18] S. De, I. Znakovskaya, D. Ray, F. Anis, N G. Johnson, I. A. Bocharova, M. Magrakvelidze, B. D. Esry, C. L. Cocke, I. V. Litvinyuk, and M. F. Kling, Phys. Rev. Lett. **103**, 153002 (2009).
[19] J. Wu and H. Zeng, Phys. Rev. A **81**, 053401 (2010).
[20] M. Muramatsu, M. Hita, S. Minemoto, and H. Sakai, Phys. Rev. A **79**, 011403(R) (2009).
[21] K. Kitano, N. Ishii, and J. Itatani, Phys. Rev. A **84**, 053408 (2011).
[22] A. Couairon and A. Mysyrowicz, Phys. Rep. **441**, 47 (2007).
[23] F. Theberge, M. Chateauneuf, G. Roy, P. Mathieu, and J. Dubois, Phys. Rev. A **81**, 033821 (2010).
[24] T.-J. Wang, J.-F. Daigle, S. Yuan, F. Theberge, M. Chateauneuf, J. Dubois, G. Roy, H. Zeng, and S. L. Chin, Phys. Rev. A **83**, 053801 (2011).
[25] J.-M. Manceau, A. Averchi, F. Bonaretti, D. Faccio, P. Di Trapani, A. Couairon, and S. Tzortzakis, Opt. Lett. **34**, 2165 (2009).
[26] S. Zhang, C. Lu, T. Jia, Z. Wang, and Z. Sun, Phys. Rev. A **83**, 043410 (2011).
[27] C. C. Shu and N. E. Henriksen, Phys. Rev. A **87**, 013408 (2013).
[28] D. Tunega and J. Noga, Theor. Chem. Acc. **100**, 78 (1998).
[29] H. Yun, H. T. Kim, C. M. Kim, C. H. Nam, and J. Lee, Phys. Rev. A **84**, 065401 (2011).
[30] T. Seideman, Phys. Rev. Lett. **83**, 4971 (1999).
[31] T. Seideman, J. Chem. Phys. **115**, 5965 (2001).
[32] D. Meshulach and Y. Silberberg, Phys. Rev. A **60**, 1287 (1999).
[33] J. Ortigoso, M. Rodriguez, M. Gupta, and B. Friedrich, J. Chem. Phys. **110**, 3870 (1999).
[34] A. Ben Haj-Yedder, A. Auger, C. M. Dion, E. Cances, A. Keller, C. Le Bris, and O. Atabek, Phys. Rev. A **66**, 063401 (2002).